2014

Thermodynamic Optimization of Tube-Fin Evaporators Operating under Frosting Conditions

Rafael S. Ribeiro
UFPR, Brazil, rafael.ribeiro@ufpr.br

Christian J. L. Hermes
UFPR, Brazil, chermes@ufpr.br

Thermodynamic Optimization of Tube-Fin Evaporators Operating under Frosting Conditions

Rafael S. RIBEIRO, Christian J. L. HERMES*

Laboratory of Thermodynamics and Thermophysics, Department of Mechanical Engineering
Federal University of Paraná, 81531990 Curitiba-PR, Brazil
* Corresponding author: chermes@ufpr.br

ABSTRACT

In this study, the method of entropy generation minimization (i.e., design aimed at facilitating both heat, mass and fluid flows) is used to improve the evaporator geometry (aspect ratio and fin density) considering the irreversibilities produced by the heat and mass transfer, and viscous flow processes. A fully algebraic semi-empirical model was put forward to simulate the thermal-hydraulic behavior of tube-fin evaporator coils running under frosting conditions. The model predictions were validated against experimental data from Silva (2012), showing a good agreement between calculated and measured counterparts, with errors within a ±5% band for the cooling capacity and the air flow rate. The optimization exercise pointed out that high aspect ratio heat exchanger designs lead to minimum entropy generation in cases of fixed heat duty and air flow rate constrained by the characteristic curve of the fan.

1. INTRODUCTION

Evaporator frosting is a major issue in most small-capacity refrigeration applications, as it depletes the evaporator capacity, thus increasing the compressor runtime needed to accomplish the same refrigerating effect required under no-frost conditions (Bejan et al., 1994; Borges et al., 2014). Favorable conditions for frost build-up over evaporator coils do require subzero surface temperatures and supercooling degrees (i.e., the temperature difference between the dew-point and the coil surface) higher than 5 K (Piucco et al., 2011).

Under frosting operation, the thermal-hydraulic characteristics of the evaporator are quite different from those observed in dry-coil conditions, as the frost layer not only imposes an extra thermal insulation (the effective conductivity of frost is ~10^3 times lower than that of the aluminum fins), but also restricts the air flow passage, thus rising the compartment temperatures, risking to spoil the goods under storage. Therefore, a proper coil design must account for the influence of geometric (e.g., number of transversal and longitudinal tubes, fin density) and operating parameters (e.g., air and coil surface temperatures, air humidity), which not only affect the heat and mass transfer rates, but also the frost growth and densification ones, which are related to the runtime until the coil gets clogged.

Tackling with such a large number of interdependent design parameters is not a simple task. In an attempt to predict the frost accretion over tube-fin evaporator coils, different simulation models have been put forward in the past decades, as summarized by Silva et al. (2011a). In general, such models assume a quasi-static growth of the frost layer, invoke the Lewis analogy for the sake of mass transfer calculations, and rely on empirical information for the frost properties, particularly the frost density (Hermes et al., 2009). The models, however, depend on the numerical integration of time-evolving differential equations, being not suitable for optimization tasks which might demand thousands of simulation runs in a row (Silva et al., 2011b).

Thermodynamic optimization of tube-fin heat exchangers, i.e. design aimed at facilitating heat and fluid flows by means of entropy generation minimization, has gained attention in the past decades (Bejan, 1987; San et al., 1987), although the optimization of tube-fin heat exchangers have been carried out considering dry-coil conditions (Hermes et al., 2012; Hermes, 2012b). There is no evidence in the open literature of a simulation model which is suitable for the thermodynamic optimization of tube-fin evaporators operating under frosting conditions. To put forward such a model is, therefore, the main aim of the present paper.

Hence, a fully algebraic model was advanced to simulate the thermal-hydraulic behavior of tube-fin evaporator coils under frosting conditions based on the first-principles of heat, mass, and momentum conservation. The closing information (e.g., Stanton number, friction factor, frost density) were obtained from experimental data from Silva (2012). After the calibration exercise, the model predictions were compared against experimental data, showing a good agreement between calculated and measured air flow rates and cooling capacities, with most errors within a ±5% band. The dimensionless entropy generation rate due to heat and moisture transfer and to viscous fluid flow was adopted as the objective function to be minimized in the process of finding out the optimum aspect ratio ($N_{tr} \times N_{lo}$) for a constrained cooling capacity.

2. ALGEBRAIC MODELING

The mathematical model was developed considering the evaporating temperature, and so the coil surface temperature are uniform allover the evaporator surface. Therefore, the air flow across the heat exchanger was modeled as an even lump, as depicted in Figure 1. In addition, bearing in mind that frost formation is a complex phenomenon, the following assumptions were taken into account (Hermes et al., 2009): (i) the moisture and heat transfer processes were regarded as quasi-static; (ii) the frost layer thickness was assumed as uniform on both the tubes and fins; (iii) the Lewis analogy was invoked for the sake of mass transfer calculations, with Le≈1; and (iv) the air properties were considered to be uniform at the control volume inlet and exit sections.

2.1 Heat and mass transfer sub-model

Since the evaporator was considered an even lump with uniform surface temperature (see Figure 1), the following heat and mass balances do apply:

$$\rho V \frac{dT}{dA_s} = \frac{kNu}{c_p D_h}(T_s - T) \tag{1}$$

$$\rho V \frac{d\omega}{dA_s} = \frac{\rho DSh}{D_h}(\omega_s - \omega) \tag{2}$$

where V is the fan-supplied air flow rate, Nu and Sh are the Nusselt and Sherwood numbers, respectively, being both based on the hydraulic diameter, $D_h=4LA_c/A_s$, T_s and $\omega_s=\omega_{sat}(T_s)$ are the temperature and humidity ratio at the frost surface, respectively, A_s is the total heat and mass transfer surface, A_c the minimum free flow passage, L the heat exchanger length in the flow direction, D the diffusivity of water vapor in air, and k and c_p are the thermal conductivity and specific heat of moist air, respectively.

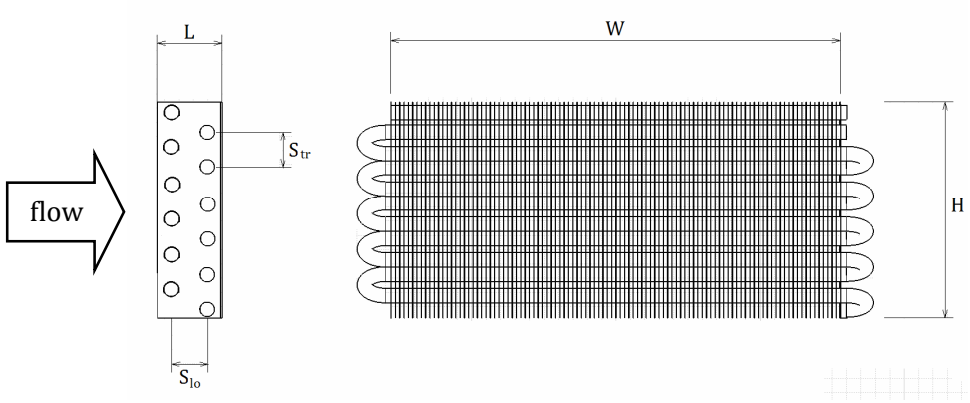

Figure 1: Schematic representation of the tube-fine evaporator. Adapted from Silva et al. (2011a,b)

Invoking the heat and mass transfer analogy, it follows that $\rho DSh=kNu/c_pLe^{2/3}$. Assuming Le≈1, one can see that equations (1) and (2) are similar, thus leading to the same solution for the temperature and humidity profiles along the air stream. Noting that $Re=\rho VD_h/\mu$ and St=Nu/RePr, where Pr is the Prandtl number, equations (1) and (2) can be solved analytically, yielding

$$\frac{T_o - T_s}{T_i - T_s} = \frac{\omega_o - \omega_{sat}(T_s)}{\omega_i - \omega_{sat}(T_s)} = \exp\left(-St\frac{A_s}{A_c}\right) \tag{3}$$

In addition, the sensible (Q_{sen}) and latent (Q_{lat}) heat transfer rates can be calculated from:

$$\frac{Q_{sen}}{c_p(T_i - T_s)} = \frac{Q_{lat}}{i_{sv}(\omega_i - \omega_s)} = \rho V\left(1 - \exp\left(-St\frac{A_s}{A_c}\right)\right) \tag{4}$$

where i_{sv} is the latent heat of sublimation. The pressure drop, on the other hand, is calculated from the following expression derived by Kays and London (1994):

$$\Delta p = p_i - p_o = \frac{f\rho}{2}\left(\frac{V}{A_c}\right)^2 \frac{A_s}{A_c} \tag{5}$$

where f is the Fanning friction factor, whereas V=V(Δp) is obtained from the fan characteristic curve. The Stanton number and the friction factor were calculated from the following correlations, derived in-house using experimental data from Silva (2012):

$$St = a_0\, Re^{a_1}\, \phi^{a_2}\, Pr^{-2/3} \tag{6}$$

$$f = b_0\, Re^{b_1}\, \phi^{b_2} \tag{7}$$

where $\phi = A_s/A_{tube}$ is the finning factor, A_{tube} the surface area of tubes only, and the a_0, a_1, a_2, b_0, b_1, b_2 coefficients were obtained from experimental data from Silva (2012).

2.2 Frost growth and densification sub-model

The frost formation sub-model is based on the approach devised by Hermes (2012a), who solved analytically the problem of frost growth and densification on flat surfaces coming up with an algebraic expression for the thickness of the frost layer as a function of the Nusselt number, and the supersaturation degree. The model was derived based on an overall mass balance in the frost layer, as follows:

$$\rho_f \frac{d\delta_s}{dt} + \delta_s \frac{d\rho_f}{dt} = \frac{Q_{lat}}{A_s i_{sv}} \tag{8}$$

In addition, an energy balance at the frost surface was also invoked, yielding

$$\left.\frac{dT}{dn}\right|_{n=\delta_s} = \frac{Q_{sen} + Q_{lat}}{k_f A_s} \tag{9}$$

where n stands for the direction perpendicular to any coil surface (tubes or fins). The model also relies on empirical information for the frost density and thermal conductivity, calculated as follows (Hermes et al., 2014):

$$\rho_f = c_0 \exp(c_1 T_f) \tag{10}$$

where c_0, c_1 and c_2 were adjusted based on data from Silva (2012), and

$$k_f = k_{fo} + \beta\rho_f \tag{11}$$

where k_{fo}=0.1312 and β=0.0003 (Hermes, 2012a).

The model was adapted to the finned-tube geometry by replacing the plate length adopted in the original formulation by the hydraulic diameter, thus yielding the following expression for the frost thickness, δ_s:

$$\frac{\delta_s}{D_h} = \frac{1}{2}\left(\left(\left(\frac{k_{fo}}{k}\frac{Ja}{Nu(1+Ja)}\right)^2 + 4(\omega_m - \omega_{sat}(T_w))\frac{k_{fo}}{k}\frac{JaFo}{1+Ja}\right)^{1/2} - \frac{k_{fo}}{k}\frac{Ja}{Nu(1+Ja)}\right) \tag{12}$$

where $Fo=kt/\rho_f c_p D_h^2$ is the modified Fourier number, $Ja=c_p(T_m-T_w)/i_{sv}(\omega_m-\omega_w)$ is the modified Jakob number, T_w is the coil temperature, and T_m and ω_m are the mean temperature and humidity ratio of the air stream, respectively, calculated from equation (3). The frost surface temperature is calculated from:

$$\frac{T_s - T_w}{T_m - T_w} = \frac{\theta}{1+\theta} \tag{13}$$

where θ was defined by Hermes (2012a) as follows:

$$\theta \equiv Nu\frac{k}{k_f}\left(1+\frac{1}{Ja}\right)\frac{\delta_s}{D_h} \tag{14}$$

Finally, the heat exchanger geometry (A_c, A_s) is determined as follows (Silva et al., 2011b):

$$A_c = WH - N_{tr}D_{ef}(W - \delta_{ef}N_{fin}) + N_{fin}\delta_{ef}H \tag{15}$$

$$A_s = \pi D_{ef}(W - \delta_{ef}N_{fin})N_{tr}N_{lo} + 2N_{fin}\left(HL - \tfrac{1}{4}\pi D_{ef}^2 N_{tr}N_{lo}\right) \tag{16}$$

where $D_{ef}=D_t+2\delta_s$, $\delta_{ef}=\delta_{fin}+2\delta_s$, D_t is the outter diameter of the tube, δ_{fin} and N_{fin} are the fin thickness and number of fins, respectively, N_{tr} and N_{lo} are the number of tubes in the transversal and longitudinal (flow) directions, respectively, and H and W are the heat exchanger height and width, respectively.

2.3 Numerical solution

The equation set is comprised of algebraic time-dependent non-linear equations which were solved simultaneously at each time-step (~1 minute) by the Newton-Raphson technique. The psychrometric properties were calculated using the formulae available from ASHRAE (1997). In this work, all thermophysical properties were evaluated for $(T_m+T_w)/2$.

3. OPTIMIZATION SCHEME

The optimization task was performed based on the method of entropy generation minimization. For conjugate heat and mass transfer, the fundamental equation of thermodynamics was invoked (Modell and Reid, 1984):

$$dH = TdS + Vdp + \tilde{\mu}_v dN_v \tag{17}$$

where $\tilde{\mu}_v$ is the chemical potential in [J mol^{-1}], and N_v is the number of mols of water in the vapor phase. The terms dH, dS and dN_v were obtained respectively from energy, entropy and water vapor mass balances, as follows:

$$dH = -(q + m\tilde{h}_v/M_v)dA_s \tag{18}$$

$$dS = -(q/T + m\tilde{s}_v/M_v)dA_s + dS_g \tag{19}$$

$$dN_v = -(m/M_v)dA_s \tag{20}$$

where q and m are the sensible heat flux and the vapor mass flux, respectively, and M_v is the molar mass of water.

Substituting equations (18) to (20) into equation (17), and writing for the entropy generation, yields

$$\frac{dS_g}{dA_s} = \frac{q}{T}\left(\frac{\Delta T}{T_w}\right) + \frac{m}{TM_v}\left(\tilde{h}_v - T\tilde{s}_v - \tilde{\mu}_v\right) + \frac{f\rho}{2T}\left(\frac{V}{A_c}\right)^3 \tag{21}$$

San et al. (1987) proposed the following approximation for small heat and mass transfer rates:

$$\tilde{h}_v - T\tilde{s}_v - \tilde{\mu}_v \approx \tilde{R}\left(\Delta T + \Delta\omega T_m/\omega_m\right) \tag{22}$$

where $\tilde{R}$ is the universal gas constant [J mol^{-1}K^{-1}]. Thus substituting eq. (22) into eq. (21), integrating over the heat exchanger area, and expressing the entropy generation in its dimensionless form, $N_s=S_g/\rho V c_p$, it follows that

$$N_s = \left(T_i - T_o\right)\frac{\Delta T}{T_w T_m} + \left(\omega_i - \omega_o\right)\frac{\tilde{R}}{M_v c_p}\left(\frac{\Delta T}{T_m} + \frac{\Delta\omega}{\omega_m}\right) + \frac{f}{2c_p T_m}\left(\frac{V}{A_c}\right)^2 \frac{A_s}{A_c} \tag{23}$$

The first term in the right-hand side stands for the entropy generation due to heat transfer, the second term is related to the mass transfer, the third term to the conjugate heat and mass transfer, and the fourth term to the viscous flow. In eq. (23), the temperature and humidity differences are calculated from logarithmic means.

4. MODEL VALIDATION

The a, b and c coefficients of equations (6), (7) and (10), respectively, were fitted using 28 experimental data points obtained from Silva (2012), who tested a frosted tube-fin evaporator under typical conditions of light commercial refrigerators: D_t=10 mm, N_{tr}=6, N_{lo}=2, N_{fin}=71, 103 and 151, δ_{fin}=2 mm, W=320 mm, H=150 mm, L=50 mm, and $S_{tr}=S_{lo}$=25 mm, running with T_w=-10°C. The characteristic curve of the fan tested by Silva (2012) is illustrated in Figure 2 and represented mathematically as follows:

$$V = \frac{d_0 + d_1\Delta p + d_2\Delta p^2 + d_3\Delta p^3 + d_4\Delta p^4 + d_5\Delta p^5}{1 + d_6\Delta p + d_7\Delta p^2 + d_8\Delta p^3 + d_9\Delta p^4 + d_{10}\Delta p^5} \tag{24}$$

where V is in [m^3/h], and Δp in [Pa]. The d-coefficients are as follows: d_0=-1.26×10^6, d_1=4.05×10^8, d_2=-3.52×10^7, d_3=10^6, d_4=-8.84×10^3, d_5=0.581, d_6=2.27×10^6, d_7=-1.41×10^5, d_8=569.2, d_9=102.4 and d_{10}=-1.315. Figure 3 shows the pumping power associated with the fan curve (VΔp), where one can note the figures do not exceed 1-W as the pumping efficiency related to electrical and mechanical losses has not been accounted for by equation (17).

The c-coefficients were firstly obtained by feeding the model with the experimental values for the cooling capacity, the air flow rate, and the frost thickness. The model was then solved reversely in order to come out with the values of frost density, which were fitted as a function of dew-point and frost surface temperature, obtaining c_0=53, and c_1=-0.159. The fitted frost density was able to represent the experimental data with errors within ±10% bounds. Once the c-coefficients were known, a second fitting procedure was carried out using cooling capacity and air flow rate data, and solved reversely in order to come out with the a- and b-coefficients for equations (6) and (7), respectively. The fitted coefficients are as follows: a_0=33, a_1=-0.82, a_2=-1.23, b_0=256, b_1=-0.82, and b_2=-1.36. The fitted equations (6) and (7) were able to represent the experimental St and f values with errors within ±5% and ±15% bounds, respectively.

Figure 4 compares the calculated and experimental cooling capacity, whereas Figure 5 does it for the air flow rate. One can see the model is able to predict the experimental counterparts with errors not exceeding ±5% bounds for most data points. The model follows the experimental trends quite satisfactorily, especially after 5-min runtime when the frost formation effects are more perceptible. It can be also noted that the heat exchanger with a large number of fins provide a higher heat duty, which is due to the higher heat transfer (finned) surface, while operating under lower air flow rates because of the increased pressure drop.

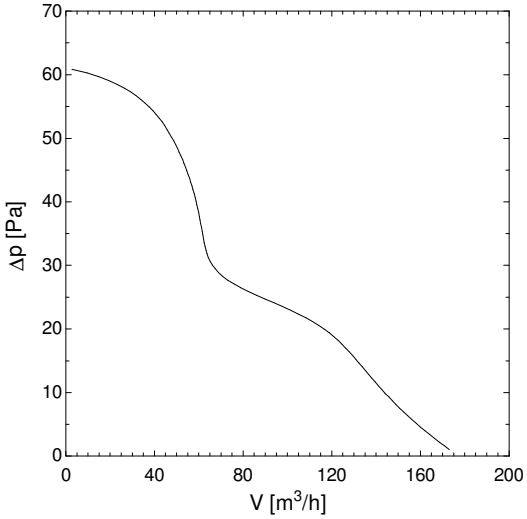

Figure 2: Characteristic curve of the fan

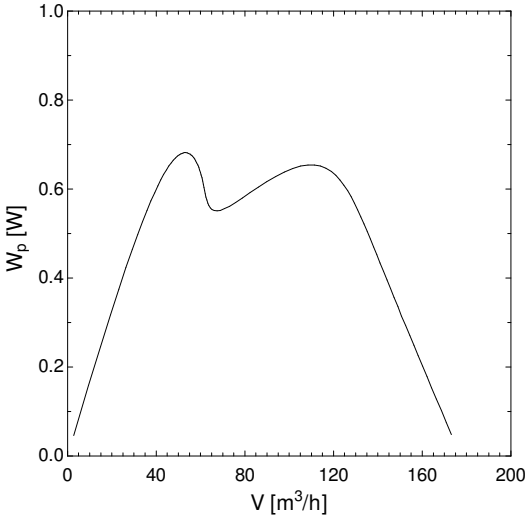

Figure 3: Pumping power associated with the fan curve

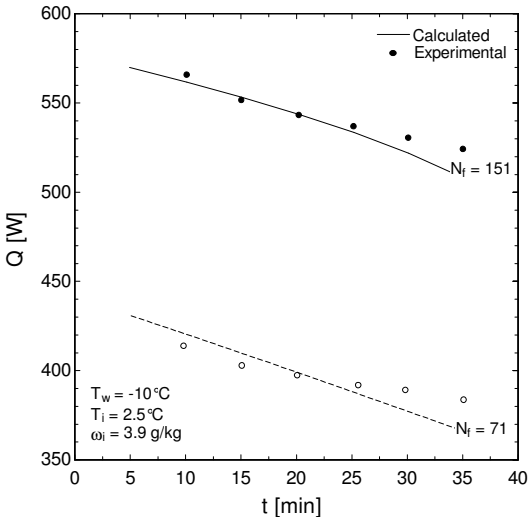

Figure 4: Comparison between calculated and measured cooling capacities

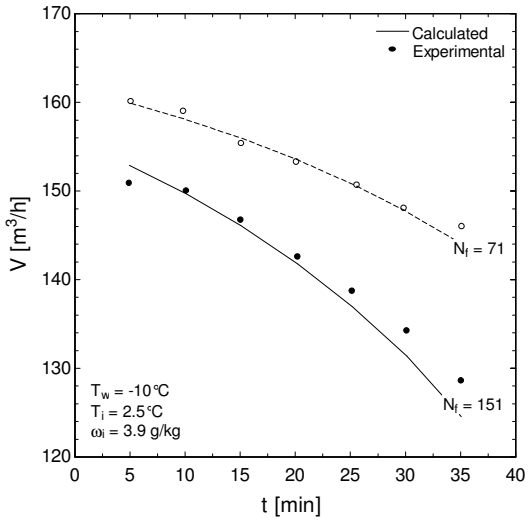

Figure 5: Comparison between calculated and measured air flow rates

5. DISCUSSION

Figure 6 illustrates equation (21) whereas Figure 7 depicts equation (23). The former expresses the rate of entropy generation per unit area, whilst the latter explores the time-evolution of the entropy generation number, which is a dimensionless parameter that relates the entropy generation to the thermal capacity of the air stream. In both cases, 71 and 151 fins were considered.

For constrained fan characteristics, it can be seen in Figure 6 that the entropy generation per unit area decreases over time, which is due to the air flow rate reduction with the pressure drop, thus diminishing the heat transfer rate inasmuch the evaporator gets frosted. The variation is more perceptible in case of 151 fins, as the pressure drop is more affected in case of smaller channels and higher heat transfer areas.

Figure 7 shows the dimensionless rate of entropy generation increases for 151 fins, but decreases for 71 fins. Such a behavior can be explained by Figures 4 and 5, which show the cooling capacities decrease at similar rates (~2 W/min for both cases), but the air flow rate decreases at higher rates for 151 fins (~1 kg/h/min) in comparison with 71 fins (~0.5 kg/h/min), which is due to the reduced free flow passage observed for the former.

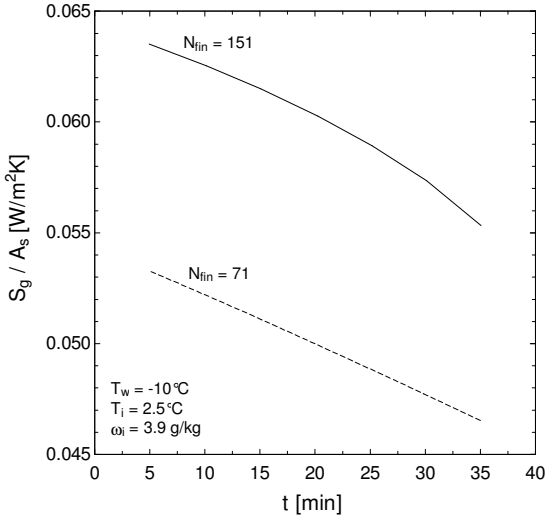

Figure 6: Time evolution of the entropy generation per unit area

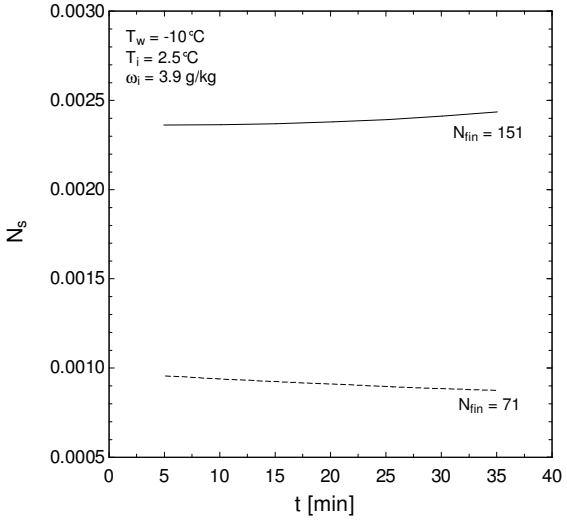

Figure 7: Time evolution of the dimensionless rate of entropy generation

Figure 8 slices up the overall rate of entropy generation into the four sources of irreversibilities accounted for by equation (23): heat transfer (q), mass transfer (m), conjugate heat and mass transfer (q × m), and friction (Δp). One can note the thermodynamic losses due to heat transfer (across finite temperature difference) play a dominant role, followed by mass transfer, viscous flow, and conjugate heat and mass transfer, being the last two practically immaterial.

Figure 9 explores the effect of the number of fins on both cooling capacity and dimensionless rate of entropy generation for a fixed aspect ratio ($N_{tr} \times N_{lo}$). In all cases, a time-averaged entropy generation rate was taken into account considering the runtime until the evaporator free flow passage is 20% of the face area. It can be seen in Figure 9 that a lower number of fins diminishes the rate of entropy generation as it depletes the cooling capacity due to a lower heat transfer area.

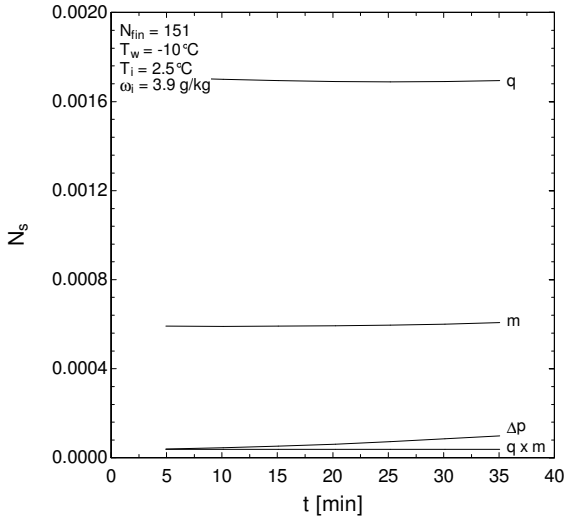

Figure 8: Individual contributions for the overall rate of entropy generation (N_{fin}=151)

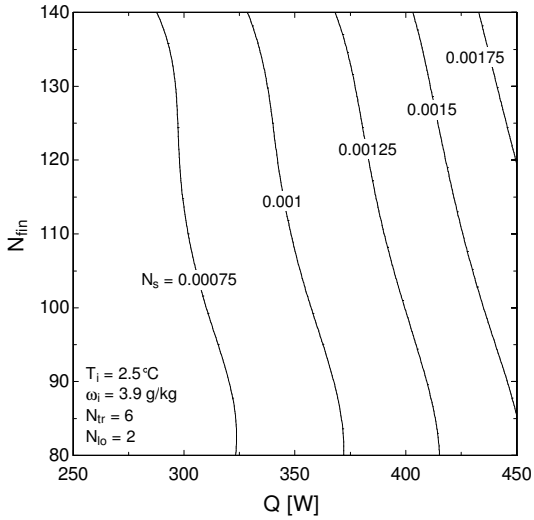

Figure 9: Dimensioless entropy generation for various N_{fin} and Q (N_{tr}=6, N_{lo}=2, T_i=2.5°C, ω_i=3.9 g/kg)

A fairer, more realistic analysis relies on keeping the cooling capacity constrained (450-W), whereas the coil temperature is free to vary. The results are depicted in Figure 10, where the numbers of transversal and longitudinal tubes were varied, whereas the number of fins was held fixed at 103. On the one hand, the analysis comes up with an

optimization path which points towards higher face areas and lower heat exchanger lengths (i.e. slender designs), thus confirming the predictions of Hermes (2012b) for no-frost conditions. On the other hand, Figure 11 shows the runtime (time until the evaporator free flow passage gets 80% blocked) diminishes in cases of slender designs, thus indicating that a higher defrost frequency might be required.

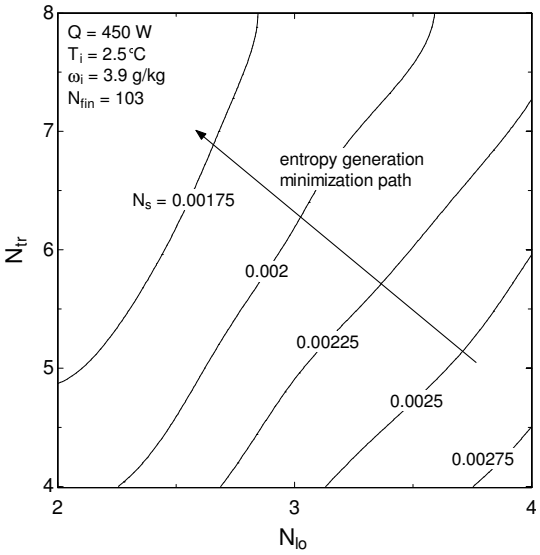

Figure 10: Dimensionless entropy generation for various aspect ratios (constrained cooling capacity)

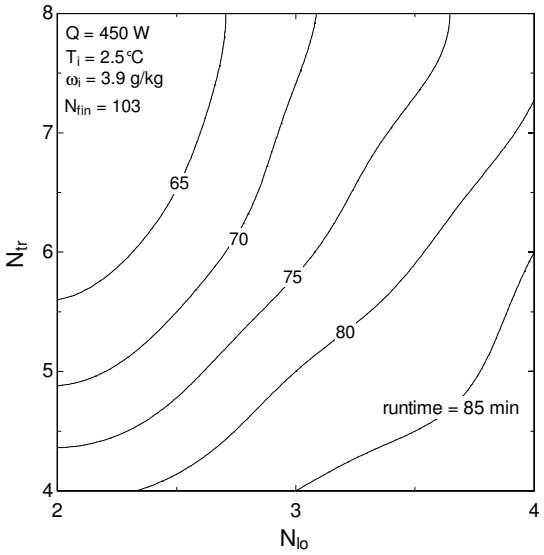

Figure 11: Runtime for various aspect ratios (constrained cooling capacity)

6. FINAL REMARKS

A fully-algebraic semi-empirical model for frost formation on tube-fin evaporator coils was proposed and validated against experimental data obtained elsewhere, where a good agreement between the experimental and calculated cooling capacities and air flow rates were observed, with errors not exceeding ±5% bounds. The dimensionless rate of entropy generation was formulated in terms of four sources of irreversibility, such as heat transfer, mass transfer, conjugated heat and mass transfer, and viscous flow. The time-averaged entropy generation rate based on the runtime until the coil gets 80% blocked was adopted as the objective function in the exercise of finding out the aspect ratio that minimizes the thermodynamic losses. It was found that high aspect ratio (i.e. slender) evaporator designs lead to lower rates of entropy generation, albeit the runtime is reduced, thus resulting into a higher defrost frequency. Therefore, there must be an aspect ratio which optimizes the overall system performance. To find out such an optimum is subject matter for further investigations.

NOMENCLATURE

Roman

A_c	minimum free flow area [m^2]
A_f	face area [m^2]
A_s	surface area [m^2]
c_p	specific heat at constant pressure [$J\ kg^{-1}K^{-1}$]
D	diffusivity of water vapor in air [$m^2\ s^{-1}$]
D_h	hydraulic diameter [m]
f	Fanning friction factor [-]
Fo	Fourier number [-]
H	height [m]
i_{sv}	frost latent heat of sublimation [$J\ kg^{-1}$]
Ja	Jakob number [-]
k	thermal conductivity [$W\ m^{-1}K^{-1}$]
L	length [m]
Le	Lewis number [-]
m	mass flux [$kg_v\ m^{-2}s^{-1}$]
N_{fin}	number of fins [-]
N_{lo}	number of longitudinal tube rows [-]
N_s	dimensionless entropy generation rate [-]
N_v	number of mols [mol]
N_{tr}	number of transversal tube rows [-]
Nu	Nusselt number [-]
q	heat flux [W/m^2]
Q	heat transfer rate [W]
S_g	entropy generation rate [$W\ K^{-1}$]
Sh	Sheerwood number [-]
St	Stanton number [-]
T	temperature [K]

V	air flow rate [m^3 s^{-1}]
W	width [m]
M_v	molar mass of water [m]
$\tilde{R}$	universal gas constant [J $mol^{-1}K^{-1}$]

Greek

δ	thickness [m]
ϕ	finning factor [-]
ρ	density [kg m^{-3}]
ω	humidity ratio [kg_v kg_a^{-1}]

Subscripts

d	densification
ef	effective frosted geometry
f	frost
fin	fin
g	growth
i	inlet
lat	latent
o	outlet
s	frost surface
sat	saturated
sen	sensible
tube	tube geometry
v	water vapor
w	coil surface

REFERENCES

ASHRAE, 1997, *Handbook of Fundamentals, American Society of Heating, Refrigerating and Air Conditioning Engineers*, Atlanta-GA, USA

Bejan A, 1987, The thermodynamic design of heat and mass transfer processes and devices, *Heat and Fluid Flow* 8, 258-276

Bejan A, Vargas JVC, Lim JS, 1994, When to defrost a refrigerator, and when to remove the scale from the heat exchanger of a power plant, *Int. J. Heat Mass Transfer* 37, 523-532

Borges BN, Melo C, Hermes CJL, 2014, Prediction of Evaporator Frosting in Household Refrigerators Subjected to Periodic Door Openings, *15th International Refrigeration and Air Conditioning Conference at Purdue*, West Lafayette-IN, USA, Paper 2219

Hermes CJL, Piucco RO, Melo C, Barbosa JR, 2009, A study of frost growth and densification on flat surfaces, *Experimental Thermal and Fluid Science* 33, 371-379

Hermes CJL, 2012a, An analytical solution to the problem of frost growth and densification on flat surfaces, *Int. J. Heat Mass Transfer* 55, 7346–7351

Hermes CJL, 2012b, Conflation of epsilon-Ntu and EGM design methods for heat exchangers with uniform wall temperature, *Int. J. Heat Mass Transfer* 55, 3812–3817

Hermes CJL, Loyola FR, Nascimento VS, 2014, A semi-empirical correlation for the frost density, *Int. J. Refrigeration*, doi: 10.1016/j.ijrefrig.2014.02.008

Hermes CJL, Silva WL, Castro FAG, 2012, Thermal-hydraulic design of fan-supplied tube-fin condensers aimed at minimum entropy generation, *App. Therm. Eng.* 36, 307-313

Kays WM, London AL, 1994, *Compact heat exchangers*, McGraw-Hill, New York, USA

Modell M, Reid RC, 1984, *Thermodynamics and Its Applications*, Prentice-Hall

Piucco RO, Hermes CJL, Melo C, 2011, In-situ evaluation of a criterion to predict frost formation on liners of refrigerated cabinets, *App. Therm. Eng.* 31, 3084-3091

San JY, Worek WM, Lavan Z, 1987, Entropy generation in combined heat and mass transfer, *Int. J. Heat Mass Transfer* 30, 1359-1369

Silva DL, 2012, *A study of frost accretion on evaporator coils and their effects on its thermal-hydraulic behavior*, DEng thesis, Federal University of Santa Catarina, Florianópolis-SC, Brazil (in Portuguese)

Silva DL, Hermes CJL, Melo C, 2011a, Experimental Study of Frost Accumulation on Fan-Supplied Tube-Fin Evaporators, *App. Therm. Eng.* 31, 1013-1020

Silva DL, Hermes CJL, Melo C, 2011b, First-principles simulation of frost accumulation on fan-supplied tube-fin evaporators, *App. Therm. Eng.* 31, 2616-2621

ACKNOWLEDGEMENT

This study was carried out under the auspices of the Brazilian funding agency CNPq.